Article

Structural-Phase Change of Multilayer Ceramics Zr-Y-O/Si-Al-N under High Temperature

Marina Fedorischeva [1,*], **Mark Kalashnikov** [1,2], **Irina Bozhko** [2], **Tamara Dorofeeva** [1] **and Victor Sergeev** [1,2]

[1]   Institute of Strength Physics and Materials Science SB RAS, 634055 Tomsk, Russia; kmp1980@mail.ru (M.K.); dorofeeva@ispms.ru (T.D.); vs@ispms.tsc.ru (V.S.)

[2]   Department of Materials Science, National Research Tomsk Polytechnic University, 634050 Tomsk, Russia; bozhko_irina@mail.ru

*   Correspondence: fed_mv@mail.ru; Tel.: +79-627-763-406

Abstract: To increase the thermocyclic resistance of material, multilayer coatings with alternating layers of Zr-Y-O and Si-Al-N were obtained via magnetron sputtering. It was established that a coating layer based on Zr-Y-O has a columnar structure; the height of the columns is determined by the thickness of the layer. The Si-Al-N-based layer is amorphous. There were monoclinic and tetragonal phases with a large lattice parameter in the composition of the Zr-Y-O-based coating layer. After high-temperature annealing, a tetragonal phase with a small lattice parameter appeared in the microscope column. In the "in situ" mode, a change in the structural state of the Zr-Y-O coating layer was detected in the temperature range of 450–500 °C; namely, a change in the grain size and coherent scattering regions, and an increase in internal elastic stresses. It was found that the thermocyclic resistance increased by more than two times for multilayer samples compared to the single-layer ones we studied earlier.

Keywords: structure-phase state; multilayer coatings; grain size; curvature torsion; phase transition; thermal cyclic resistance

1. Introduction

Heat-protective coatings based on ZrO_2-Y_2O_3 are used in the production of gas turbine engines (GTE) to protect from the effects of the high temperature of the main components: combustion chambers, nozzle and turbine blades, etc. Such coatings also effectively protect the metal base of the GTE blades from high-temperature overloads, oxidizing, erosive and corrosive effects of the aggressive environment (gases) formed during the combustion of the fuel, and also allow one to effectively deal with the problems that determine the reliability, operability and the working life of structures, equipment, etc. [1–6].

Ceramic materials based on partially stabilized zirconium dioxide have unique properties: high bending strength and crack resistance in combination with chemical inertia and hardness, which makes them widely in demand as structural and functional ceramics [7,8].

It is known that zirconium dioxide ZrO_2 has three stable crystal structures that depend on temperature: a monoclinic structure below 1200 °C, a tetragonal structure between 1200 °C and 2370 °C and a cubic structure above 2370 °C. The mechanical properties of ceramics based on zirconium dioxide are known to be the function of the phase composition and the structure. Tetragonal zirconium dioxide has high strength and toughness. Various methods and technologies have been improved for the production and stabilization of the tetragonal phase in zirconium dioxide materials. The most common method has become the formation of tetragonal zirconium dioxide by adding stabilizing impurities to it. Analysis of the literature data has shown that yttrium oxide Y_2O_3 is most often used as a stabilizing impurity, which inhibits the transformation of the tetragonal phase into the monoclinic one during cooling.

The ZrO_2-Y_2O_3 ceramics system based on the tetragonal modification of zirconium dioxide (t-ZrO_2) has the highest mechanical characteristics, which, in accordance with the state diagram at normal pressure, exists in the temperature range of 1200–2370 °C [8,9]. Alloying of zirconium dioxide with 3–5 mol.% Y_2O_3 makes it possible to preserve the high-temperature tetragonal phase in the metastable state up to room temperature [10–14]. The high-temperature phases of zirconium dioxide have high physical and mechanical properties, which contribute to the great interest in this material. The presence of the monoclinic–tetragonal transition is accompanied by a sharp increase in volume, which leads to the destruction of ZrO_2 products. To ensure the possibility of using ZrO_2, it is necessary to stabilize high-temperature modifications in the entire temperature range up to room temperature. It is also known that diffusion and diffusion-free phase transformations occur in zirconium dioxide ceramics depending on the stabilizing impurities, the pressure, the temperature, the ambient gas environment, the humidity and the time of their exposure [15–20], which lead to significant changes in the phase composition, the structure and the mechanical properties of the above material.

For example, stabilization of zirconium dioxide with up to 6 mole% erbium (Er_2O_3), samarium (Sm_2O_3) or neodymium (Nd_2O_3) leads to stable t'-ZrO_2. The compounds Cr_2O_3-ZrO_2 and Al_2O_3-ZrO_2 decompose into m- and t-phases after heat treatment, and Cr_2O_3-ZrO_2 retain a stable t'-ZrO_2 phase [21]. In the work of Shen [22], the rare earth elements erbium and yttrium were used for alloying. The use of these elements in various ratios has led to an increase in the number of the cycles during thermocyclic tests. It is interesting to note that the number of cycles during thermal cycling for the Y-ZrO_2 coating remains the maximum. This value is comparable with the YEr-ZrO_2 coating. The authors explain the improvement of the thermal conductivity and the thermal cyclical resistance through the ability of the alloying elements to lead to a non-transformable tetragonal t' ZrO_2 phase. In other words, the joint alloying of Y and Er leads to a columnar microstructure and a relatively good thermal insulation ability, which may be responsible for the long service life of the Y-Er-ZrO_2 TBS under thermal shock. In [23], a thermal barrier coating doped with ZrO_2-$YO_{1.5}$-NbO_2 is considered. The addition of niobium contributed to a significant decrease in the thermal conductivity by about 52% compared to zirconium dioxide with a molar content of yttrium of 7.6%.

A study of the above phenomena allows one to better understand the nature of phase transformations, as well as to learn how to control its properties and even predict the ceramics' behavior.

The aim of this study was to study the structural and phase states of multilayer nanocomposite coatings based on alternating heterogeneous Zr-Y-O and Si-Al-N layers and to trace the processes occurring in the coating structure under heating in the "in situ" mode via TEM and X-ray, and also to investigate the thermal cycling of the multilayer coating at high temperatures.

2. Materials and Methods

The deposition of the coating was produced using the «KVANT-03MI» equipment [24] with two magnetrons using mosaic zirconium–yttrium and aluminum–silicon targets. The surface of the substrate was polished up to the roughness Ra = 0.16 μm before ionic treatment by Ti ions. The magnetron was powered from a pulse source with a frequency of 50 kHz. The sample was placed in the chamber on a rotating table, which could be moved in different directions—in front of the ion source for ion bombardment, and then in front of the magnetron for deposition of a coating. The substrate bias potential was −900 V under the bombardment of the surface layer of the substrate and −100 V during the deposition of a coating.

The fine structure of the multilayer coatings was investigated via transmission electron microscopy (TEM) using the JEM-2100 device (Japan). A foil was prepared via the «cross-section» method using the ION SLISER-EM-09100IS installation. The grain structure of the coatings was investigated in the temperature range of 25–900 °C in the microscope column

and the vacuum camera of the XRD-7000S device in the «in situ» mode. The secant method was used to determine the grain size [25]. Another method for determining the grain size which was used in this study was the method of estimating the average grain size of ultrafine materials by the number of reflections on the Debye rings of the microdiffraction patterns obtained by TEM. This technique is described in detail in [26,27]. The authors propose using the correlation curve to relate the continuity of the diffraction rings to the average size of the grains that form the diffraction reflections.

The curvature torsion (indicating the presence of internal elastic stresses) was determined using the parameters of the bending extinction contours observed in the TEM images of the coating material. This technique is described in detail in [27–30].

The structural-phase state was studied via X-ray using the DRON-7 device (Burevestnik, Russia, "NANOTECH" ISPMS SB RAS). X-ray investigation of the coatings was carried out under continuous 2θ scanning with Bragg–Brentano focusing in Co Kα radiation. The high-temperature X-ray analysis was carried out using the XRD-7000S X-ray diffractometer (Shimadzu, Japan) with a high-temperature prefix. The sample was heated in a high-temperature chamber for 25 min to the desired temperature. Then, the sample was cooled spontaneously together with the chamber to RT. A tungsten–rhenium thermocouple was used to control the temperature. The database JCPDS PDF-4 was used to interpret the diffractograms. Structural characteristics, such as the crystalline lattice parameter, the size of the coherent scattering regions, and the phase composition were determined by the methods described in [31]. The resistance of the coatings to cracking and peeling when changing the temperature was determined from the results of thermal cycling of the samples according to the following regime: heating the sample to 1000 °C for 1 min, then forced cooling for 1 min to a temperature of 20 °C, photographing the surface of the sample on the side of the coating using a special Microscope DCM500 camera on an optical microscope BMG-160 (Carl Zeiss, Oberkochen, Germany), the data being transferred directly to the computer, then heating again. The total duration of each cycle, including all the stages of the process—heating, cooling, photographing—was 5 min. Photographing of the coating was also carried out before testing for thermal cycling resistance. For the criterion of the thermal stability of the coatings, the number of the cycles until the detachment of 50% of the coating area from the sample surface was selected. After that, the tests were stopped. The thermal cycling resistance is described in detail in [32].

3. Results

Figure 1 shows the TEM image of the cross-section of a multilayer coating based on the Zr-Y-O/Si-Al-N. The layers of the multilayer coating were found to consist of the elements Zr, Y, O, Si, Al, and N. Figure 1b shows the results of the EDS in the selected area of the transverse cross-sections of the coating and the distribution of the elements over the multilayer coating (the area of study is highlighted with a red rectangle). We can see that the thickness of the single layer is about 1000 ± 100 nm.

In Figure 2, one can see the TEM image of the structure of a multilayer coating consisting of the alternating Si-Al-N and Zr-Y-O layers of equal thickness. The darker contrast has a layer on the basis of Zr-Y-O. The lighter contrast has a layer based on the Si-Al-N.

The results of TEM studies of the structural-phase state of the Zr-Y-O coatings in cross-section are presented in Figure 2. The light-field images (Figure 2d) clearly show that the coating has a crystalline columnar structure. The crystals in the form of columns are oriented perpendicular to the surface of the substrate and extend over the entire thickness of the formed coatings. This columnar structure is one of the characteristic features of coatings obtained via pulsed magnetron deposition.
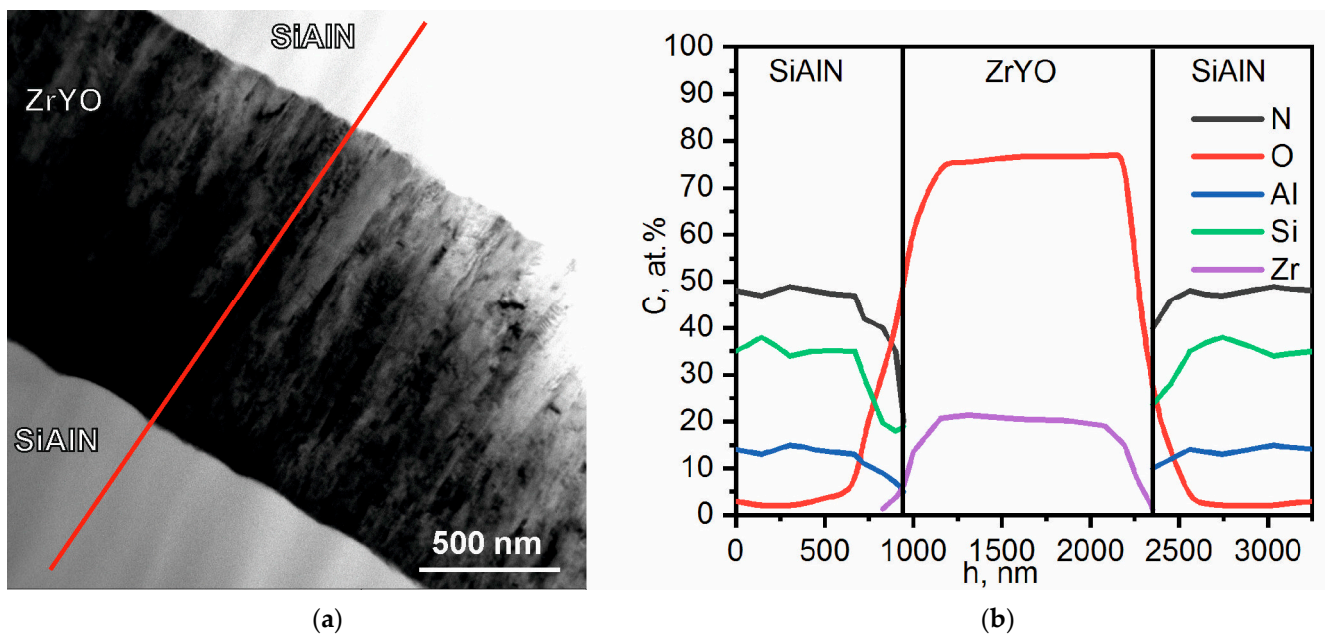
(a) **(b)**

Figure 1. Cross-sections of the TEM images of the multilayer coatings on the basis of Zr-Y-O/Si-Al-N with a thickness of individual layers about 1000 ± 100 nm: bright-field image (**a**), depth distribution of the elements (**b**).

Microdiffraction patterns (Figure 2c) of the Zr-Y-O coatings are a set of ring reflexes. The identification of the microdiffraction patterns presented in Figure 2j–l shows that under pulsed magnetron deposition, zirconium dioxide ZrO_2 is formed in the coatings of the Zr-Y-O system in the monoclinic and tetragonal modifications. It should be noted that the ring reflexes in the indicated microdiffraction pattern consist of a large number of closely spaced point reflexes. This type of microdiffraction pattern allows one to assert that the Zr-Y-O coating has a crystal structure with a small size of structural elements. A detailed study of the bright-field and dark-field electron microscopic images reveals that as the Zr-Y-O coating grows, the transverse dimensions of its crystallites increase. Thus, the results of the measurements have allowed us to establish that the average transverse size of the crystallites of this coating near the substrate is about 25–30 nm, and near the next layer, the average size of the crystallites increases and is about 80 nm.

As for the layer based on Si-Al-N, it is amorphous. This is evidenced by the microdiffraction patterns in Figure 2a which are typical for an amorphous material.

The same picture shows the TEM images of the multilayer coatings based on Zr-Y-O in the initial state (d), at a temperature of 900 °C (e) and after cooling in a high-temperature chamber (f), the microdiffraction patterns in the nanodiffraction mode corresponding to the selected areas (g–i) and the ring microdiffraction from the visible area (j–l).

It was found using TEM that the structure of the layer based on Zr-Y-O in the Zr-Y-O/Si-Al-N multilayer coating contains the tetragonal and monoclinic phases in the initial state and at a temperature of 900 °C. In the Zr-Y-O coating layer after cooling, the tetragonal phase t′ with a small crystal lattice parameter (a = 3.64 Å, c = 5.27 Å) was found, which was not observed in the initial state and at 900 °C. It is known that the above phase, in contrast to the tetragonal t-phase, does not undergo reversible phase transformations [33] of the tetragonal and monoclinic phases.

It is also known that the stability of the tetragonal phase, which is the most preferable for operations under extreme conditions, depends on the grain size. The larger the grain size the faster the phase transition from the high-temperature tetragonal phase to the monoclinic one [33]. Therefore, the grain size is an important characteristic of a material operating at high temperatures. The effect of temperature on the grain size of the ZrO_2 layer in the Si-Al-N–Zr-Y-O multilayer coating is discussed further in detail.
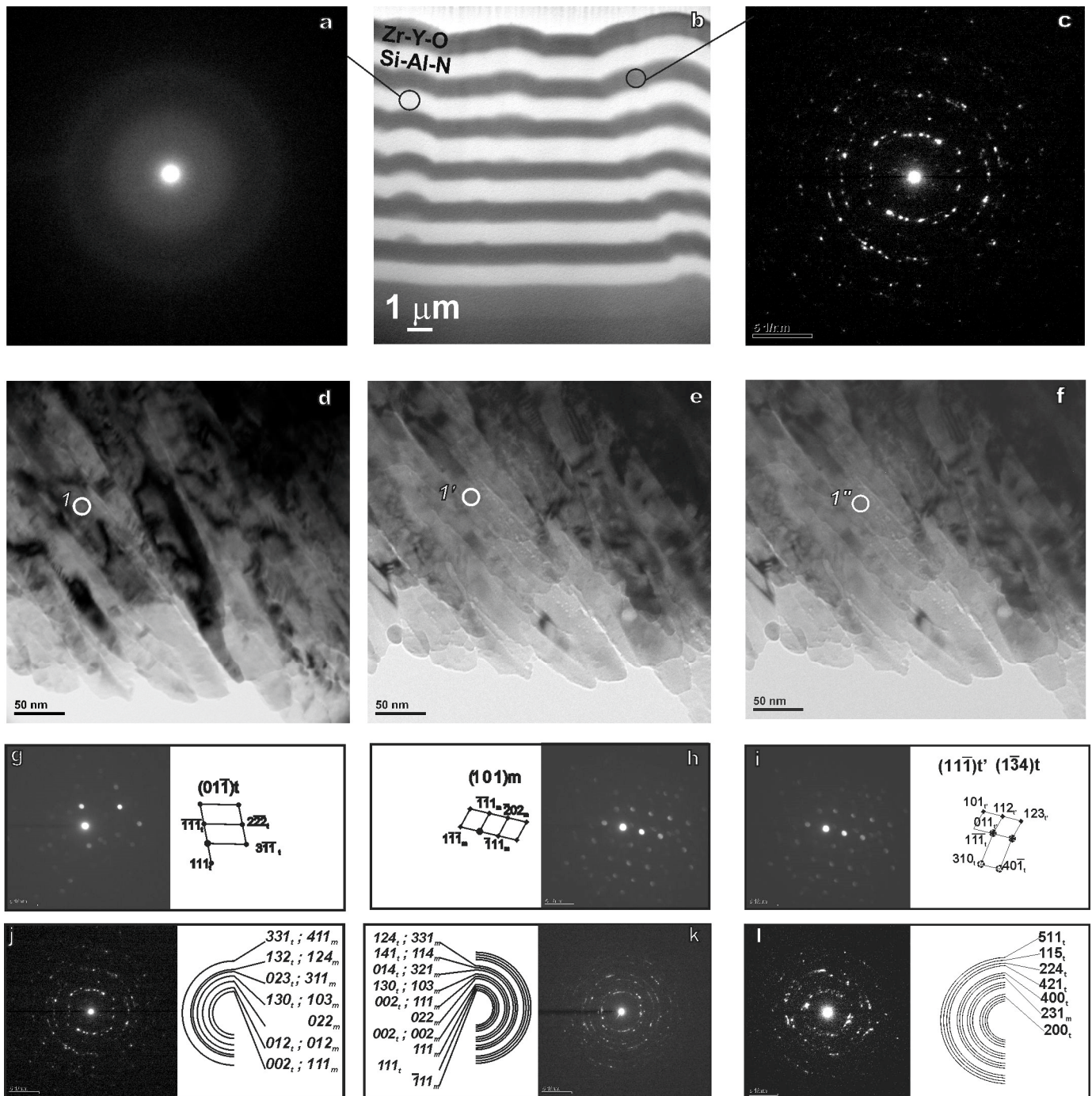
Figure 2. TEM image of the cross-section of the protective coatings of the Zr-Y-O-Si-Al-N system obtained by pulsed magnetron sputtering: alternating layers (**b**); the microdiffraction patterns of the amorphous layer on the basis of Si-Al-N (**a**); the ring microdiffraction of the layer Zr-Y-O (**c**); the bright field of the layer Zr-Y-O in the initial state (**d**) and at a temperature of 900 °C (**e**) and after cooling (**f**); the microdiffraction patterns in the nanodiffraction mode from the circled area (**g,h,i**), from the visible area (**j,k,l**) and the indexing scheme, respectively.

Further, the changes occurring at temperatures from room temperature to 900 °C were investigated. First, the sample was heated from room temperature to 400 °C for 30 min. Similar heatings were carried out at temperatures of 450 °C, 475 °C, 600 °C and 900 °C.

Figure 3 presents the microdiffraction patterns and the grain size distributions of the coating layer based on Zr-Y-O for the above temperatures. As can be seen, all the grain size

distributions for all temperatures are unimodal and close to normal. The average grain size in the initial sample is about 15 nm. When it was heated up to 400 °C, the distribution became noticeably blurred and the most probable values shifted to the region of the large grain size, with the average grain size increased up to 20 nm.
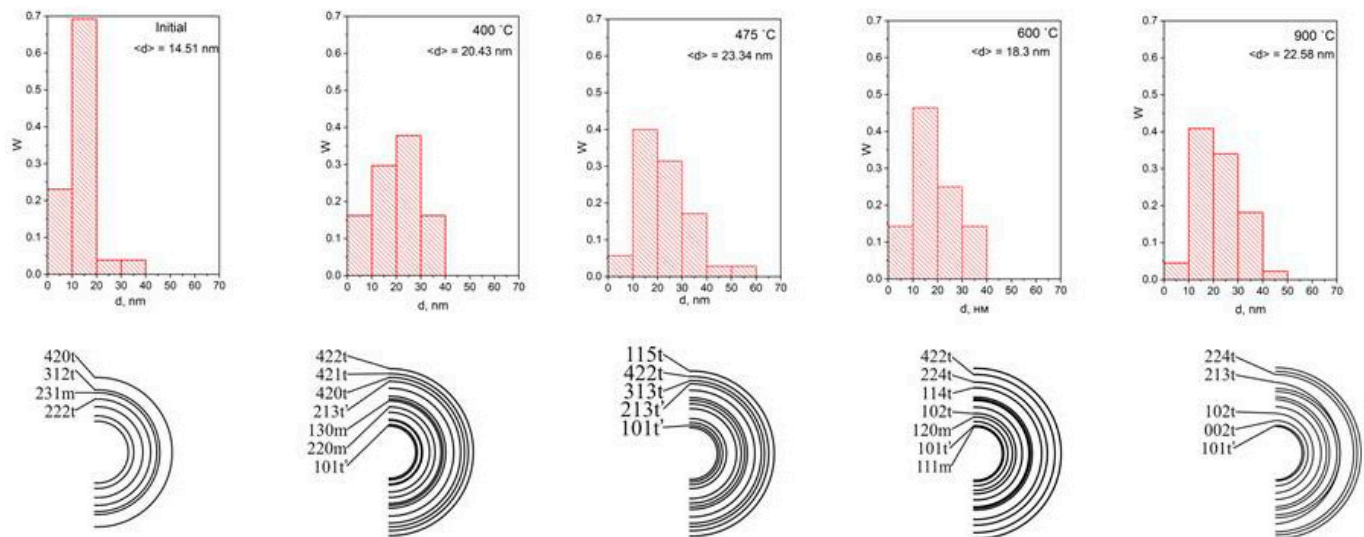

Figure 3. The grain size distribution of the coating based on Zr-Y-O for different temperatures (shown in the figures), the corresponding microdiffraction patterns and the indexing scheme.

The number of small grains significantly reduced. With a further increase in temperature, the fraction of the small grain size (less than 10 nm) decreased and the regions with a large (up to 60 nm) grain size appeared. The distribution had an asymmetric shape: there was a small "tail" in the region of the large grain size. In this case, the most probable grain size of about 20 nm remained at the level of the initial state almost up to 900 °C. The proportion of the grains with a minimum grain size of less than 10 nm was the smallest at temperatures of 475 °C and 900 °C.

Let us try to interpret the results in Figure 3. Judging by the blurring of the image of the distribution at 400 °C, recrystallization first occurs with an increase in the average grain size to about 20 nm. A further increase in temperature to 475 °C leads to a maximum increase in the average grain size to 23 nm, and in this case, the maximum blurring of the grain size distribution is observed, which suggests that at the above temperature, the martensitic phase transition from the tetragonal phase to the monoclinic one occurs most actively [1]. It is known that a method that stabilizes the high-temperature phase at room temperature is the introduction of impurity ions (in our case, yttrium) into the crystal lattice, which produces local compression regions. In this case, solid solutions are formed with stabilizer oxides, whose cations are larger than the zirconium ions and cause local compressive stresses [34–37].

A decrease in the concentration of the stabilizing ion in the bulk of the material can be responsible for the phase transformation of the tetragonal phase into the monoclinic one. It is known that with an increase in temperature, the rate of atoms diffusing, including those of the alloying elements, increases, with the atom migrating to the grain boundaries [37]. This leads to the fact that the number of the local compression regions in the solid solution decreases and, consequently, the stabilizing effect of yttrium on the crystal lattice of the ZrO_2 tetragonal phase decreases.

An increase in the amount of the monoclinic phase, which has a larger volume (according to various sources, from 4% to 9%) compared with the tetragonal one, leads to an increase in the internal elastic stresses [33,37,38]. As is known, the internal elastic stresses lead to a phase transition (from a tetragonal to a monoclinic one) in this system. The relaxation of these stresses takes place, according to the dislocation model, due to the

formation of dislocations followed by the formation of a grain–subgrain structure. This is evidenced by a decrease in the internal elastic stresses and a decrease in the grain size of the structure at 600 °C and high temperature [39].

Table 1 shows the values of the curvature torsion of the crystal lattice, which characterizes the internal elastic stresses of the coating layer in the Zr-Y-O/Si-Al-N multilayer coating. The components of the internal stress tensor were reconstructed from the parameters of the bending extinction contours observed in the TEM images of the coating layer. It can be seen that the maximum value of the curvature torsion of the material occurs at a temperature range of 450 °C–475 °C.

Table 1. Grain size determined by secant and diffraction patterns, coherent scattering blocks and values of the curvature torsion of the crystal lattice in the coating layer based on Zr-Y-O at different annealing temperatures.

Temperature, (°C)	Average Value of the Transverse Grain Size, nm (TEM)	Average Grain Size by Microdiffraction, nm (TEM)	Size of Coherent Scattering Units (X-ray)	Average Value of Curvature of Torsion χ, (cm^{-1}) (TEM)
Initial	15 ± 2	20 ± 2	26 ± 2	2.51
400	20 ± 2	24 ± 2		3.28
450	22 ± 2	26 ± 2	37 ± 2	4.27
475	23 ± 2	22 ± 2		3.82
600	19 ± 2	19 ± 2		2.02
900	23 ± 2	22 ± 2		1.82
1000	-	-	25 ± 2	
1100			26 ± 2	
1300			35 ± 2	
1400			37 ± 2	
25			36 ± 2	

It is known that in a substrate coating system (in our case, coating–coating layers), internal elastic stresses always arise. During heating, the internal energy of the system changes. This process is caused by changes in any system and is accompanied by the change in the phase composition, grain growth, etc. With increasing temperature, two competing processes take place: the appearance of thermal stresses and their relaxation [33].

Presumably, in our case, up to temperatures of 400–500 °C, the internal energy is accumulated, which leads to an increase in the transverse size of the grains, and, consequently, to the curvature torsion of the crystal lattice (emergence of stresses). Next, the martensitic transition of the tetragonal phase to the monoclinic one (the relaxation stage) starts. In [33,37], the authors observed a martensitic phase transition at a temperature of 500 °C for YSZ coatings with an yttrium content of up to 3 mol%.

Further, the grain size decreases until the temperature of 600 °C is reached, and then it gradually increases up to 1400 °C (X-ray), remaining unchanged after cooling. Evidently, a large quantity of t'-ZrO$_2$ is contained in the Zr-Y-O coating, which stabilizes coating structure.

The data of the X-ray studies confirm the data of the electron microscopy. Figure 4a shows the fragments of the X-ray patterns of the coating layer based on Zr-Y-O. It can be seen that with an increase in the heating temperature, the reflexes of the X-ray diffractograms shift to the left which indicates an increase in the internal elastic stresses (Figure 4a). At room temperature after cooling together with the camera, the X-ray peaks return to their initial position. At the same time, the width at half-height also changes, which indicates a change in the coherent scattering regions. Indeed, their size is maximum at a temperature of 450 °C, i.e., the main trend remains: the grain size measured by two methods (TEM) and the size of the coherent scattering regions (X-ray) increases in the temperature range of 400–500 °C. In this regard, the curvature torsion of the crystal lattice (χ) increases, indicating an increase in the internal elastic stresses (TEM) at the same temperatures. Figure 4b

shows the dependences of the grain size determined by two methods: the size of the coherent scattering regions and the curvature of the torsion of the crystal lattice. It can be seen that all the features (a sharp increase in the grain size, an increase in the internal elastic stresses) take place within the temperature range of 400–500 °C.
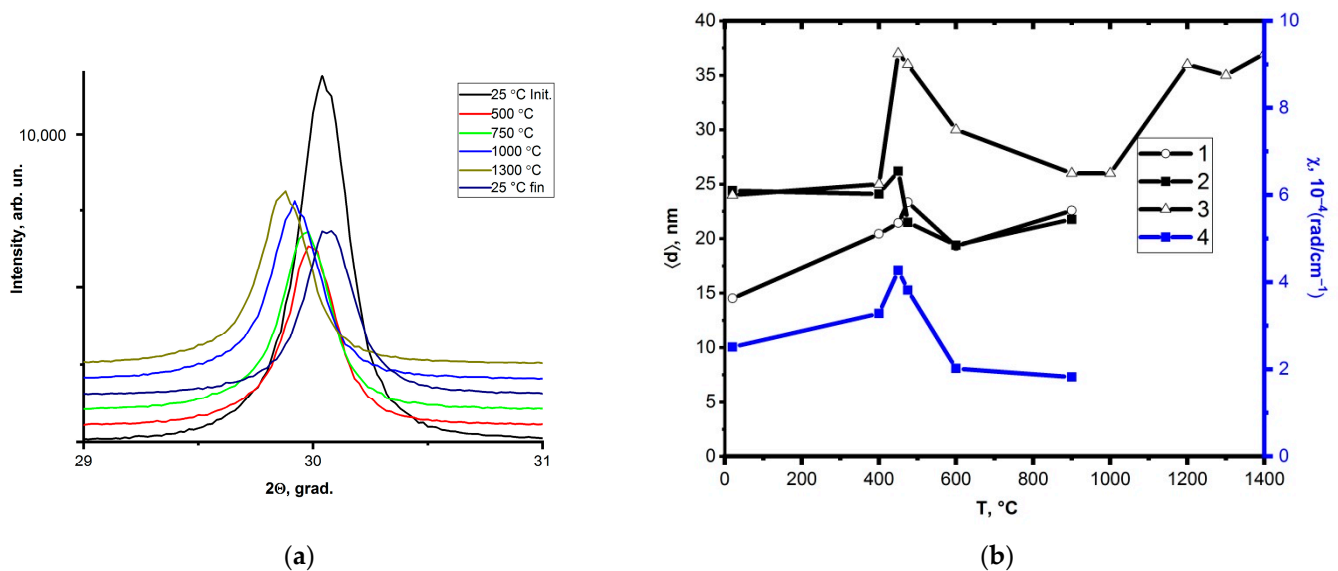

Figure 4. Fragments of the X-ray patterns obtained at temperatures from room temperature to 1300 °C (**a**), the dependence of the coherent scattering blocks (curve 1), the grain size (curves 2, 3) and the curvature torsion of the crystal lattice on temperature (curve 4) (**b**).

Thermocyclic resistance of the multilayer Zr-Y-O/Si-Al-N coatings was researched.

For the criterion of the thermal stability of the coatings, the number of the cycles before the destruction of 50% of the coating area of the sample surface was selected [32]. After that, the tests were stopped. Figure 5 shows that half of the coating will peel off only after 95 cycles in the multilayer coatings.

This value is significantly higher than that for the single-layer coating studied in [32].

The higher values of the thermocyclic resistance of a multilayer coating based on Zr-Y-O/Si-Al-N compared to a single-layer Zr-Y-O are caused by the presence of the Si-Al-N intermediate layer.

The intermediate layer is the main carrier of mechanical loads and relaxes the amplitude stresses arising during thermal cycling in a multi-level coating. It has high strength, high crack resistance and resistance to thermal shock, high relaxation ability and a low coefficient of thermal expansion. Si-Al-N-based ceramics meet all these requirements. The introduction of the intermediate layer under thermal cycling allows for a "multilayer coating-substrate" system, reducing the amplitude values of thermal compression–tension stresses in the upper functional layer. As a result, the decrease in the crack braking effect observed at high temperatures due to weakening of the mechanism of transformational hardening of yttrium-stabilized zirconium dioxide can be partially or completely compensated [40].
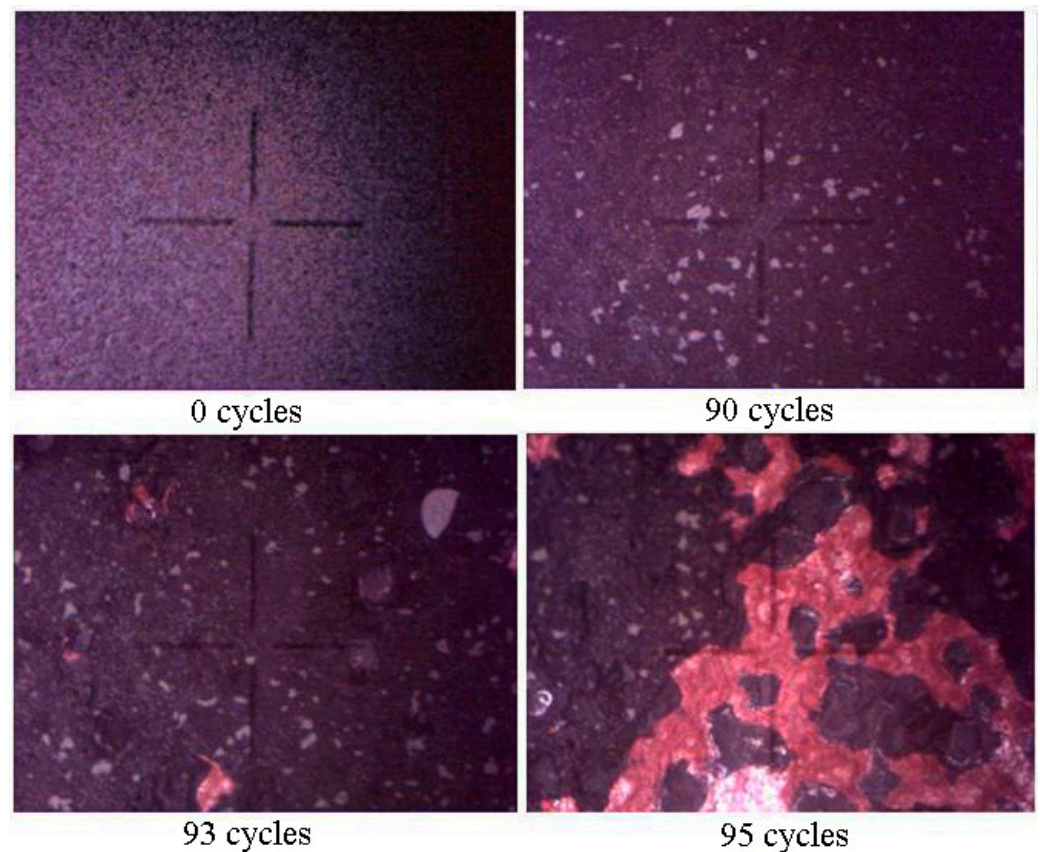
Figure 5. Optical images of the heat-shielding surface coatings on the basis of the Zr-Y-O/Si-Al-N coating obtained under thermocyclic resistance test (the dimension of the observed field is 2.09 × 1.56 mm).

4. Conclusions

Thus, pulsed magnetron sputtering was used to form multilayer nanostructured coatings based on the Zr-Y-O/Si-Al-N systems with alternating layers with a total coating thickness of ~10 μm. It was established by TEM and X-ray methods that the Zr-Y-O layers contain the ZrO_2 phases in the tetragonal and monoclinic modifications. The layers based on Zr-Y-O in the multilayer coating of Zr-Y-O/Si-Al-N have a columnar structure, with the size of the columns in the cross-section reaching 80 nm and the height of the columns being about 1000 nm, which, in this case, corresponds to the thickness of the applied layer. The structure of the Si-Al-N-based layers is amorphous.

During high-temperature TEM studies in the "in situ" mode in the Zr-Y-O layer of a multilayer coating based on Zr-Y-O/Si-Al–N in the temperature range of 400–500 °C, the grain size and the coherent scattering regions change. As a result, internal elastic stresses appear, leading to the martensitic phase transformation.

After cooling, the tetragonal phase t'-ZrO_2 with a small crystal lattice parameter (a = 3.64 Å c = 5.27 Å) was detected in the Zr-Y-O coating layer, which was not observed in the initial state and at 900 °C.

Thermocyclic resistance of the multilayer Zr-Y-O/Si-Al-N coatings is about two times higher than that of a single-layer coating. This is due to the presence of the Si-Al-N intermediate layer, which has a high crack resistance and a resistance to thermal shock, a high relaxation ability and low coefficient of thermal expansion.

References

1. Yasuda, K.; Goto, Y.; Takeda, H. Influence of Tetragonality on Tetragonal-to-Monoclinic Phase Trans-formation during Hydrothermal Aging in Plasma-Sprayed Yttria-Stabilized Zirconia Coatings. *J. Am. Ceram. Soc.* **2020**, *84*, 1037–1042.

2. Langjahr, P.A.; Oberacker, R.; Hoffmann, M.J. Long-Term Behavior and Application Limits of Plasma-Sprayed Zirconia Thermal Barrier Coatings. *J. Am. Ceram. Soc.* **2001**, *84*, 1301–1308. [CrossRef]

3. Gruninger, M.F.; Boris, M.V. Thermal Barrier Ceramics for Gas Tur-bine and Reciprocating Heat Engine Applications. In *Thermal Spray: International Advances in Coatings Technology*; Berndt, C.C., Ed.; ASM International: Almere, The Netherlands, 1992; pp. 487–492.

4. Soechting, F.O. A Design Perspective on Thermal Barrier Coatings. In Proceedings of the Thermal Barrier Coating Workshop, NASA CP-33, Westlake, OH, USA, 27–29 March 1995; Volume 12, pp. 1–15.

5. Bose, S.; Demasi-Marcin, J. Thennal Barrier Coating Experience inGas Turbine Engine at Pratt & Whitney. In Proceedings of the Thermal Barrier Coating Workshop, NASA CP-3312, Westlake, OH, USA, 27–29 March 1995; pp. 63–73.

6. Tanaka, M. Ion- and electron-beam-induced structural changes in cubic yttria stabilized zirconia. *Appl. Phys. A* **2018**, *124*, 647. [CrossRef]

7. Sinitsyn, D.Y.; Anikin, V.N.; Eremin, S.A.; Yudin, A.G. Protective coatings based on ZrO_2-Y_2O_3 and Al_2O_3–TiO_2 systems with modifying additives on CCCM. *Refract. Ind. Ceram.* **2017**, *58*, 194–201. [CrossRef]

8. Zhigachev, A.O.; Golovin, Y.I.; Umrikhin, A.V.; Korenkov, V.V.; Tyurin, A.I.; Rodaev, V.V.; Dyachek, T.A. *Ceramic Materials Based on Zirconium Dioxide*; Golovin, Y.I., Ed.; Technosfera: Moscow, Russia, 2018; 358p.

9. Stubican, V.S.; Hink, R.C.; Ray, S.P. Phase Equilibria and Ordering in the System ZrO_2-Y_2O_3. *J. Am. Ceram. Soc.* **1978**, *6*, 17–21. [CrossRef]

10. Lyakishev, N.P. (Ed.) *Diagrams of Binary Metallic Systems*; Mashinostroenie: Moscow, Russia, 1997.

11. Kulkov, S.N.; Buyakova, S.P. Phase composition and features of structure formation based on stabilized zirconium dioxide. *Russ. Nanotechnol.* **2007**, *2*, 119–132.

12. Lughi, V.; Sergo, V. Low Temperature Degradation -Aging- of Zirconia: A Critical Review of the Relevant Aspects in Dentistry. *Dent. Mater.* **2010**, *8*, 807–820. [CrossRef]

13. Chevalier, J.; Gremillard, L.; Virkar, A.V.; Clarke, D.R. The Ttetragonal-Monoclinic Transformation in Zirconia: Lessons Learned and Future Trends. *J. Am. Ceram. Soc.* **2009**, *92*, 1901–1920. [CrossRef]

14. Eichler, J.; Rodel, J.; Ulrich, E.; Mark, H. Effect of Grain Size on Mechanical Properties of Submicrometer 3Y-TZP: Fracture Strength and Hydrothermal Degradation. *J. Am. Ceram. Soc.* **2007**, *90*, 2830–2836. [CrossRef]

15. Hannink, R.H.; Kelly, P.M.; Muddle, B.C. Transformation Toughening in Zirconia-Containing Ceramics. *J. Am. Ceram. Soc.* **2000**, *83*, 461–487. [CrossRef]

16. Zhou, K.; Xie, F.; Wu, X.; Wang, S. Fretting wear behavior of nano ZrO_2 doped plasma electrolytic oxidation. *Surf. Coat. Technol.* **2021**, *421*, 127429. [CrossRef]

17. Borik, M.A.; Kulebyakin, A.V.; Myzina, V.A.; Lomonova, E.E.; Milovich, F.O.; Ryabochkina, P.A.; Sidorova, N.V.; Shulga, N.Y.; Tabachkova, N.Y. Mechanical characteristics, structure, and phase stability of tetragonal crystals of ZrO_2-Y_2O_3 solid solutions doped with cerium and neodymium oxides composite coatings on TC21 titanium alloy. *J. Phys. Chem. Solids* **2021**, *150*, 109908. [CrossRef]

18. Pang, E.L.; Olson, G.B.; Schuh, C.A. Schuh, The mechanism of thermal transformation hysteresis in ZrO_2-CeO_2 shape-memory ceramics. *Acta Mater.* **2021**, *213*, 116972. [CrossRef]

19. Kablov, E.N.; Muboyadzhyan, S.A. Heat-resistant and heat-shielding coatings for turbine blades high-pressure promising gas turbine engines. *Aviat. Mater. Technol.* **2012**, *1*, 60–70.

20. Tamarin, Y. *Protective Coatings for Turbine Blades USA*; ASM International: Almere, The Netherlands, 2002; pp. 3–300.

21. Boissonnet, G.; Chalk, C.; Nicholls, J.R.; Bonnet, G.; Pedraza, F. Phase stability and thermal insulation of YSZ and erbia-yttria co-doped zirconia EB-PVD thermal barrier coating systems. *Surf. Coat. Technol.* **2020**, *389*, 125566. [CrossRef]

22. Shen, Z.; Liu, Z.; Mu, R.; He, L.; Liu, G. Y–Er–ZrO$_2$ thermal barrier coatings by EB-PVD: Thermal conductivity. *Appl. Surf. Sci. Adv.* **2021**, *3*, 100043. [CrossRef]

23. Takahashi, J.M.K.; Assis, F.; Piorino Neto, D.A.P. Reis Thermal conductivity study of ZrO$_2$-YO$_{1.5}$-NbO$_{2.5}$ TBC. *J. Mater. Res. Technol.* **2022**, *19*, 4932–4938. [CrossRef]

24. Sergeev, V.P.; Yanovsky, V.P.; Paraev, Y.N.; Kozlov, S.A.; Zhuravlyov, S.A. Installation of ion magnetron sputtering of nanocrystalline coatings "KVANT". *Phys. Mesomech.* **2004**, *7*, 333–336.

25. Saltykov, S.A. *Stereometric Metallography*; Metallurgy: Moscow, Russia, 1970.

26. Morris, D.G.; Morris, M.A. Microstructure and Strength of Nanocrystalline Copper Alloy prepared by mechanical Alloying. *Acta Met.* **1991**, *39*, 1763–1770. [CrossRef]

27. Ivanov, Y.F.; Kozlov, E.V. Electron microscopic analysis of nanocrystalline materials. *Phys. Met. Met. Sci.* **1991**, *7*, 206–208.

28. Korotaev, A.D.; Tyumentsev, A.N. Physical Design Principles of Thermally Stable Multicomponent Nanocomposite Coatings. *Phys. Mesomech.* **2023**, *26*, 137–151. [CrossRef]

29. Kozlov, E.V. Structure and Resistance to Deformation of UFG Metals and Alloys. In *Severe Plastic Deformation*; Altan, B.S., Ed.; Nova Science Publishers, Inc.: New York, NY, USA, 2005; pp. 295–332.

30. Panin, V.E.; Panin, A.V.; Elsukova, T.F.; Popkova, Y.F. Fundamental role of crystal structure curvature in plasticity and strength of solids. *Phys. Mesomech.* **2015**, *18*, 89–93. [CrossRef]

31. Gorelik, S.S.; Rastorguev, L.N.; Skakov, Y.A. *X-ray and Electron-Optical Analysis*; Metallurgy: Moscow, Russia, 1994; pp. 124–127.

32. Fedorischeva, M.; Kalashnikov, M.; Bozhko, I.; Sergeev, V. Influence of the structural-phase state of a copper substrate upon modification with titanium ions on the thermal cyclic resistance of a coating based on Zr-Y-O. *Metals* **2022**, *12*, 65. [CrossRef]

33. Akimov, G.Y.; Timchenko, V.M.; Gorelik, I.V. Specific features of phase transformations in finely dispersed zirconium dioxide deformed by high hydrostatic pressure. *FTT* **1994**, *36*, 3582–3585.

34. Trunec, M. Effect of Grain Size on Mechanical Properties of 3Y-TZP Ceramics. *Ceram. Silik.* **2008**, *52*, 165–171.

35. Scott, H.G. Phase relationships in the zirconia-yttria system. *J. Mater. Sci.* **1975**, *10*, 1527–1535. [CrossRef]

36. Zhu, W.; Nakashima, S.; Marin, E.; Gu, H.; Pezzotti, G. Microscopic mapping of dopant content and its link to the structural and thermal stability of yttria-stabilized zirconia polycrystals. *J. Mater. Sci.* **2020**, *55*, 524–534. [CrossRef]

37. Akimov, G.Y.; Marinin, G.A.; Kameneva, V.Y. Evolution of the phase composition and physical and mechanical properties of ceramics ZrO$_2$+4mol.% Y$_2$O$_3$. *Phys. Solid State* **2005**, *47*, 2060–2062. [CrossRef]

38. Stark, D. *Diffusion in Solid*; Trusov, Energy: Moscow, Russia, 1980; p. 239.

39. Perevalova, O.B.; Konovalova, E.V.; Koneva, N.A.; Kozlov, E.V. *Effect of Atomic Ordering on Grain Boundary Ensembles of FCC Solid Solutions*; Portnova, T.C., Ed.; NTL Publisher: Tomsk, Russia, 2014; p. 250.

40. Sergeev, V.P. *Kinetics and Mechanism of the Formation of Nonequilibrium States of Surface Layers under Conditions of Magnetron Sputtering and Ion Bombardment*; Lyachko, N.Z., Psahie, S.G., Eds.; Nanoengineering Surface; Publishing House of the SB RAS: Novosibirsk, Russia, 2008; pp. 227–276.